CHAPTER- IV

Structural Studies Using Synchrotron X-ray Powder Diffraction Data and its Correlation with Dielectric Properties

4.1 Introduction

In the previous chapter, we tried to settle the room temperature crystal structure of BF-xPFN using laboratory source x-ray diffraction data. The laboratory x-ray diffraction data creates more complexity because of the presence of $CuK\alpha_2$ contributions. Further, Rietveld refinement results using laboratory source x-ray diffraction data for the cubic compositions region reveal very high values for the isothermal parameters (B_{iso}), specifically for the A-site and O-site ions. The high amplitude of the thermal parameters for A-site and O-site ions indicate that ions are locally shifted from their ideal cubic positions while maintaining the average cubic structure. Besides the anomalously high value for the isotropic thermal parameters, there are other observations which suggest that the 'cubic' phase is not ideally cubic: (i) temperature dependent dielectric plot for x = 0.40 shows evidence for a ferroelectric transition [Buhrer, (1962)], (ii) *P-E* hysteresis loop have been reported for 2% La doped BF-0.8PFN composition [Paik et al. (2009)] (iii) it had been reported that BF-0.8PFN shows a peak at 365 K in heat capacity versus temperature curve due to a ferroelectric phase transition [Bhat et al. (1974)]. This transition temperature is the same as reported by Krainik et al. (1965) using temperature dependent dielectric study.

In order to capture local displacements of A-site and O-site ions, we require high energy synchrotron x-ray powder diffraction data so that we can

obtain accurate thermal parameters. To address these issues, we have collected high energy and high resolution synchrotron x-ray diffraction data for some of the representative compositions of BF-xPFN solid solution. In this chapter, we present the results of Rietveld refinement using high energy synchrotron x-ray diffraction data for selected compositions of BF-xPFN taking into account the possibility of local displacements of cations/anions while preserving the average cubic symmetry. The structural instabilities in ferroelectrics are always linked with the change in dielectric constant at the phase transition temperature or composition [Blinc and Zeks (1974)]. In this chapter we also report the results of room temperature dielectric measurements on BF-xPFN samples in the entire composition region to locate the anomalies at the MPBs discussed in the previous chapter and the present chapter.

4.2 Experimental

Different compositions of BF-xPFN solid solutions were synthesized by the method described in chapter II. For the dielectric measurements, BF-xPFN pellets were smoothly polished with 0.25 μm diamond paste and then washed with acetone to clean the pellets surface. Isopropyl alcohol was then applied to the polished surface for removing the moisture, if any, on the pellets surface. Fired-on silver paste was subsequently applied on both the faces of the pellets. It was first dried at 150°C in an oven and then cured by firing at 500°C for about 2 min. The temperature dependent dielectric measurements at various frequencies in the range 500 Hz-1MHz were carried out at a heating rate of 1 K/min using a Novo control (Alpha-A) high performance frequency analyzer.

High-energy synchrotron x-ray powder diffraction experiments were performed using a large Debye–Scherrer camera equipped with an imaging plate as a two dimensional detector installed at the BL02B2 beam line in SPring-8 at a wavelength of 0.4110 Å for room temperature measurements [Nishibori et al. (2001)]. We collected high resolution synchrotron x-ray powder diffraction data for the compositions with x = 0.3, 0.35, 0.40, 0.50, 0.70, 0.80, 0.90 and 0.96. The high-energy synchrotron x-ray powder diffraction data were analyzed by Rietveld technique using FULLPROF software package [Carvajal et al. (2010)]. It was necessary to consider anisotropic peak broadening as per Stephen's model introduced in FULLPROF package [Stephen's (1999)].

4.3 Results and Discussion

4.3.1 Evolution of synchrotron x-ray diffraction profiles with composition

Fig. 4.1 depicts the evolution of 222_{pc}, 400_{pc} and 440_{pc} (all the reflections are written in terms of doubled pseudocubic (pc) perovskite cell) peak profiles of high resolution synchrotron x-ray diffraction patterns with compositions (x). The room temperature crystal structure of BF-0.3PFN is rhombohedral with R3c space group as evident from the characteristic splitting of the 222_{pc} and 440_{pc} pseudocubic reflections in agreement with our results of the previous chapter. The 440_{pc} reflection is doublet for BF-0.3PFN while it is a triplet for BF-0.35PFN composition.

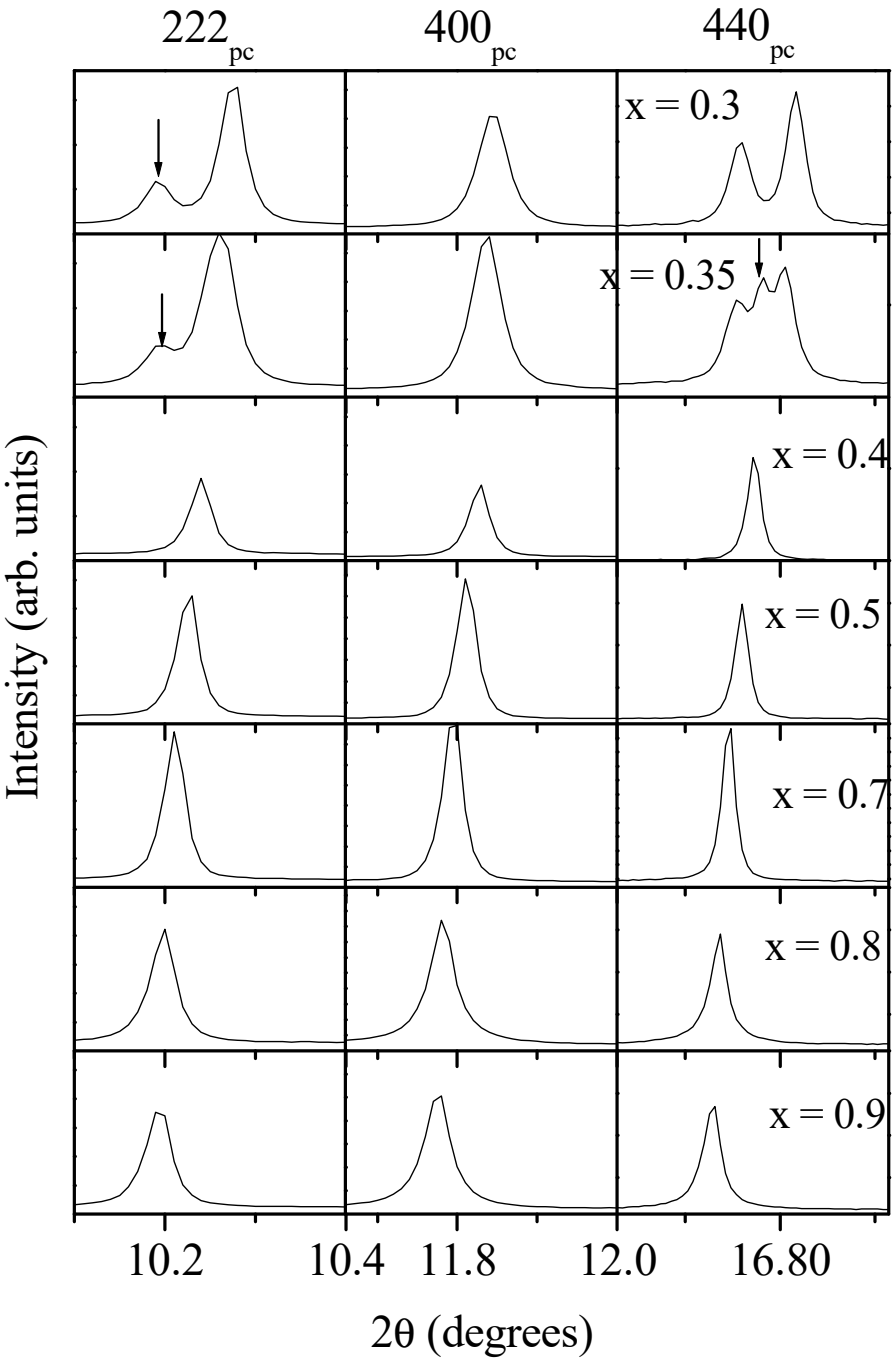

Fig. 4.1 Evolution of 222_{pc}, 400_{pc} and 440_{pc} synchrotron x-ray diffraction profiles for various compositions of BF-xPFN with x = 0.3, 0.35, 0.4, 0.5, 0.7, 0.8 and 0.9 at room temperature. Arrow(s) for 222_{pc} indicate the doublet nature of peak profile while for the 440_{pc} indicates the triplet nature of the peak profile.

The peak position of middle peak of triplet 440_{pc} of BF-0.35PFN matches with the peak position of singlet 440_{pc} for BF-0.4PFN composition. This confirms co-existence of two phases in the R3c and cubic $Pm\bar{3}m$ space groups in agreement with our results of previous chapter. Further, all the three pseudocubic reflection in the composition region $0.4 \leq x < 0.96$ are singlet. This was not obvious from Fig. 3.1 of the previous chapter due to incomplete removal of $K\alpha_2$ contribution using our software and also because of the presence of asymmetry on the lower 2θ side of the 222_{pc} peak due to slit functions. Fig. 4.2 depicts the variation of FWHM (full width at half maximum) of 400_{pc} and 444_{pc} pseudocubic reflections with composition. The FWHM of 400_{pc} reflection for the BF-0.35PFN is ~ 0.041 which sharply drops to ~ 0.027 for BF-0.4PFN at the first MPB corresponding to rhombohedral to cubic phase transition. The anomalous peak broadening of 400 for x=0.35 is partially due to the co-existence of two phases for this composition and partially due to large anisotropic strains as confirmed by the more broadening of 400_{pc} of 0.3 as compared to that for $0.40 \leq x < 0.96$. The FWHM of 400_{pc} and 444_{pc} pseudocubic reflections decreases with increasing x up to BF-0.7PFN composition and then abruptly shoots up at $x \approx 0.8$.

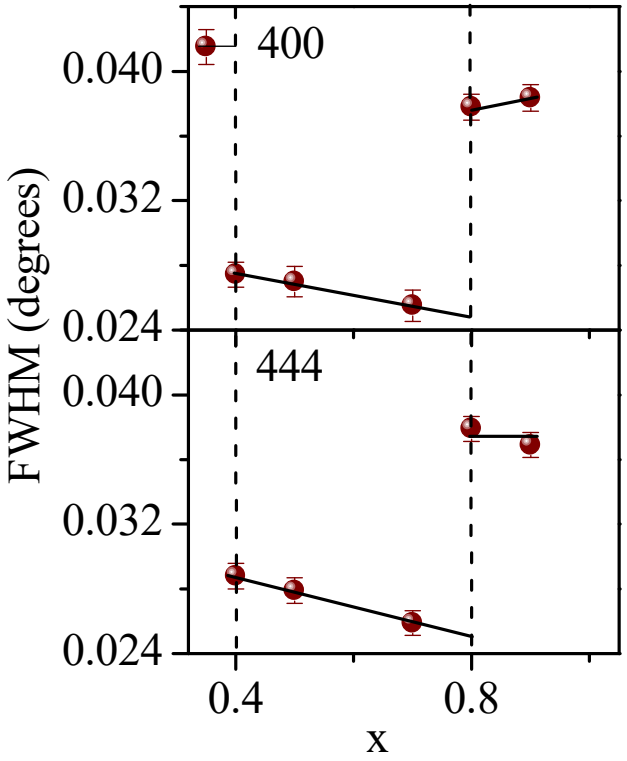

Fig. 4.2 Variation of the FWHM (full width at half maximum) with composition for the 400 and 444 pseudocubic peaks obtained by least square fitting of the respective reflections. Reflections are written in terms of doubled pseudocubic perovskite cell.

The change in the FWHM from its value in the composition region $0.40 \leq x \leq 0.70$ to its value for $x \geq 0.8$ indicates subtle changes in the local structure of the cubic phase. With this quantitative background, we now proceed to carry out Rietveld refinements taking into account the local disorder of cations and anions in the cubic phase. Before we present the Rietveld results, we also provide evidence for ferroelectric transition in the cubic compositions using dielectric measurements.

4.3.2 Evidence for ferroelectric transition in dielectric measurements

Fig. 4.3 depicts the variation of the real ($\varepsilon^{/}$) and imaginary ($\varepsilon^{//}$) parts of the dielectric constant with temperature at a fixed frequency of 900 kHz. This frequency was chosen to capture the intrinsic dielectric contributions from the grains free from extrinsic contributions (grain boundaries and electrodes etc) which occur at lower frequencies [Singh et al. (2008)]. It is evident from this figure that all the compositions, including those showing 'cubic' structure exhibit a peak in $\varepsilon^{/}$ corresponding to a ferroelectric phase transition. The variation of ferroelectric phase transition temperature (T_C) with composition is shown in Fig. 4.4 which suggests that T_C decreases with increasing PFN content. This is expected since the T_C of PFN is ~ 385 K where as T_C of BF is ~1103 K [Plantov et al. (1970), Smolenskii et al. (1958b), Kaczmarek and Pajak (1975)].

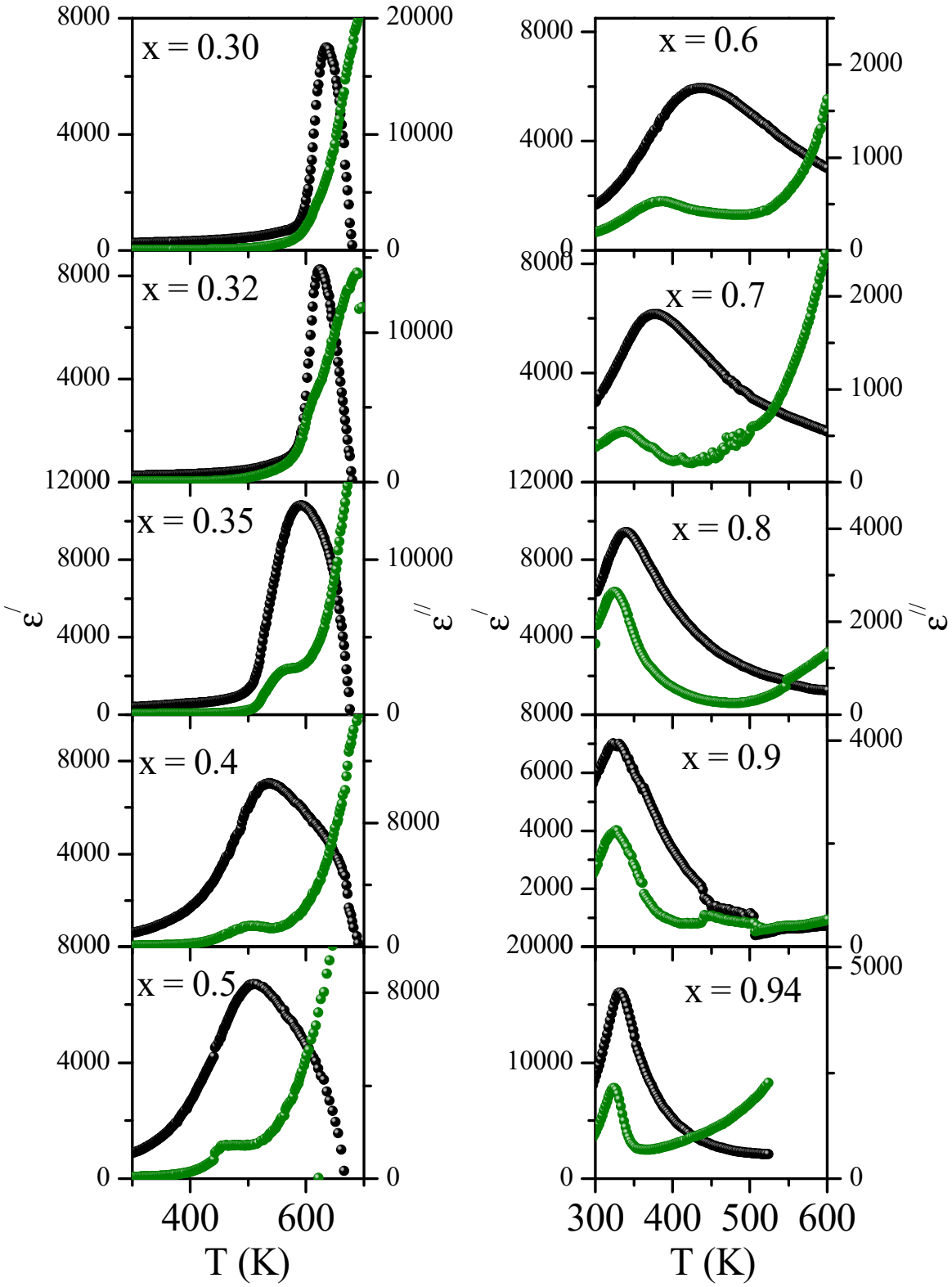

Fig. 4.3 Variation of the real ($\varepsilon_r^{/}$) and imaginary ($\varepsilon_r^{//}$) part of the dielectric constant with temperature for BF-xPFN solid solution measured at 900 kHz frequency.

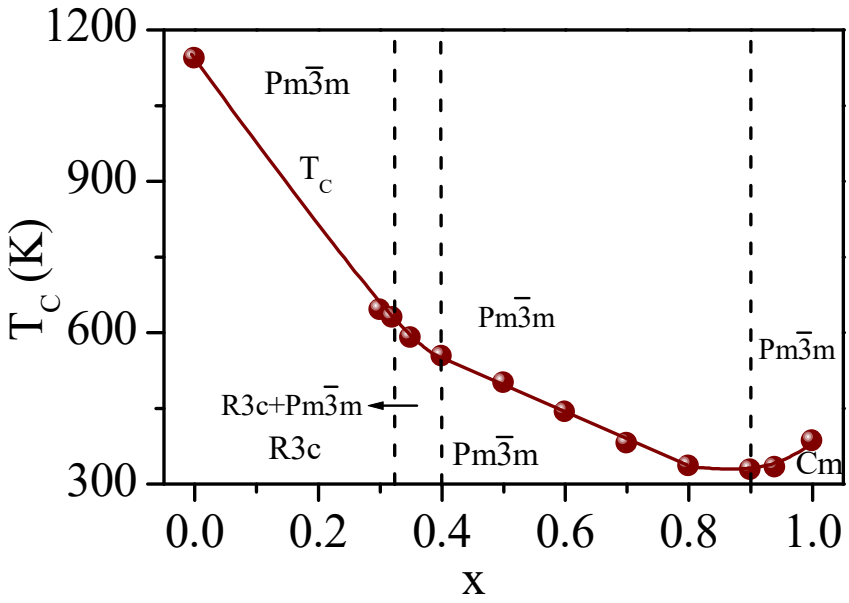

Fig. 4.4 Composition (x) variation of ferroelectric transition temperature (T_C) of BF-xPFN.

4.3.3 Rietveld Refinement of different crystallographic phases of BF-xPFN

4.3.3.1 Rietveld refinement of BF-0.3PFN

The room temperature crystal structure of BF-0.3PFN was shown to be rhombohedral with R3c space group by using laboratory x-ray diffraction data in the previous chapter. Therefore, the initial unit cell and atomic position parameters obtained by Rietveld refinement in the previous chapter were used for the refinement. Assuming pseudo-Voigt type peak profile function and linear interpolation for background modeling, the refinement soon converged, giving profile fitting parameters R_{wp} = 3.99, R_{exp} = 4.80 and χ^2 = 0.69. The refined isotropic thermal parameters (B_{iso}) for Bi^{3+}/Pb^{2+}, Fe^{3+}/Nb^{5+} and O^{2-} are

3.35, 0.75 and 2.48 $Å^2$ respectively. Use of anisotropic thermal parameters for Bi^{3+}/Pb^{2+} improve fit with R_{wp} = 3.78, R_{exp} = 4.80 and χ^2 = 0.62. The anisotropic thermal parameters for Bi^{3+}/Pb^{2+} are found to be (β_{11}) = 0.038 $Å^2$ and (β_{33}) = 0.003 $Å^2$ which reveal disc-shaped anisotropic displacement ellipsoid. The high values of isotropic thermal parameter for Bi^{3+}/Pb^{2+} and disc-shaped anisotropic displacement ellipsoid with $\beta_{11} > \beta_{33}$ indicate local shift of Bi^{3+}/Pb^{2+} ions from the ideal position in a direction perpendicular to the three fold axis of the rhombohedral unit cell. The observed, calculated and difference profiles for BF-0.3PFN are shown in Fig. 4.5 for the anisotropic thermal parameter. The refined unit cell parameters and atomic positions are given in Table 4.1.

4.3.3.2 Rietveld refinement of BF-xPFN for $0.40 \leq x \leq 0.70$

The qualitative analysis of high energy and high resolution synchrotron x-ray diffraction data shows that all the reflections are singlet in the composition region $0.40 \leq x \leq 0.70$ suggesting cubic structure. However, since a tetragonal phase with P4mm space group has also been proposed in literature for such compositions [Buhrer, (1962)], we considered both cubic with space group $Pm\bar{3}m$ and tetragonal with space group P4mm structural models in the refinements for the above mentioned composition range. The refinement was initially carried out assuming isotropic (B_{iso}) temperature parameters.

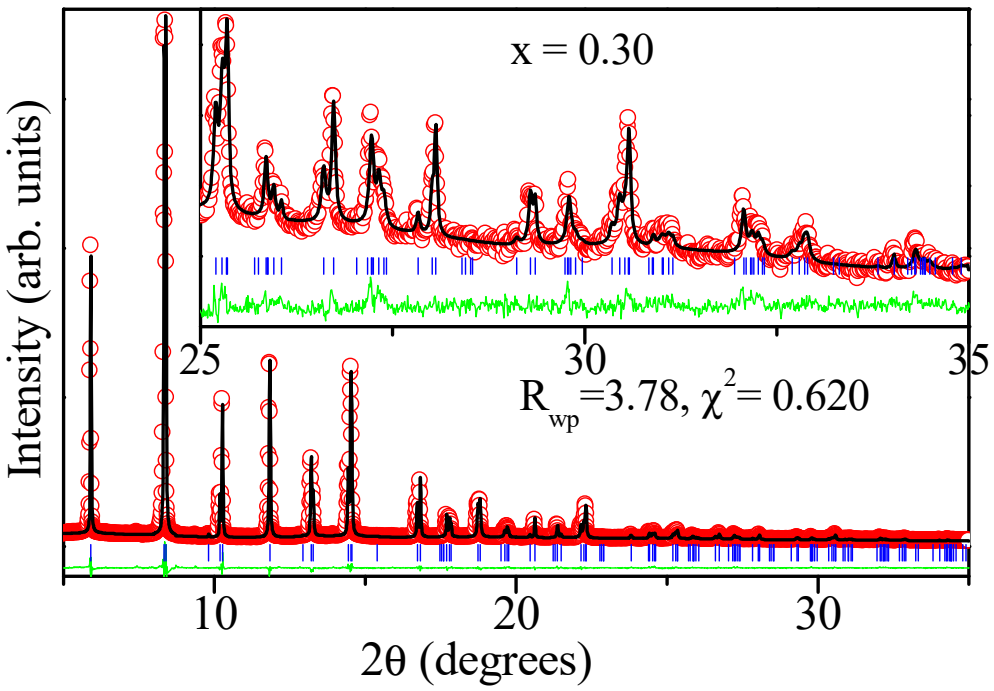

Fig. 4.5 Observed (dots), calculated (solid line), and difference (bottom line) patterns obtained from Rietveld analysis of the room temperature synchrotron x-ray diffraction data of BF-xPFN for x = 0.30. The vertical tick marks above the difference pattern stand for the Bragg peak positions. The inset depicts the fit for high-angle reflections on a magnified scale.

Fig. 4.6 shows the results of Rietveld refinements for BF-0.4PFN which was taken as a representative composition for the range $0.40 \leq x \leq 0.70$. The agreement factors for P4mm and $Pm\bar{3}m$ are found to be $R_{wp} = 4.68$, $\chi^2 = 0.547$ and $R_{wp} = 4.55$, $\chi^2 = 0.509$, respectively. The cubic model with $Pm\bar{3}m$ space group gives slightly better refinement fit in comparison with tetragonal model with P4mm space group inspite of lesser number of refinable parameters. This clearly rules out the tetragonal P4mm space group. The absence of any splitting in the 400_{pc} and 440_{pc} peak in Fig. 4.1 also rejects the tetragonal space group.

However, the isotropic thermal parameter (B_{iso}) for the Bi^{3+}/Pb^{2+} ions are very large for both the structural models (~ 5.86 $Å^2$ for $Pm\bar{3}m$ and ~ 6.1 $Å^2$ for P4mm). The high values of B_{iso} for Bi^{3+}/Pb^{2+} are usually ascribed to local displacements, which may be either static or dynamic. The B_{iso} for O^{2-} ion is also very large (~ 3.7 $Å^2$). For both the structural models, mismatch in intensities was found for those reflections which fulfilled h + k + l = odd condition, where h, k and l are pseudocubic Miller indices. This type of mismatch between observed and calculated profiles has also been reported in PZT ($PbZr_{1-x}Ti_xO_3$) [Zhang et al. (2011), Kuroiwa et al. (2005)]. Our results also suggest that the A-site and O-site ions are displaced from their ideal cubic positions. Therefore, cubic model with local disorder was used for the refinement of BF-xPFN in composition range $0.40 \leq x \leq 0.70$.

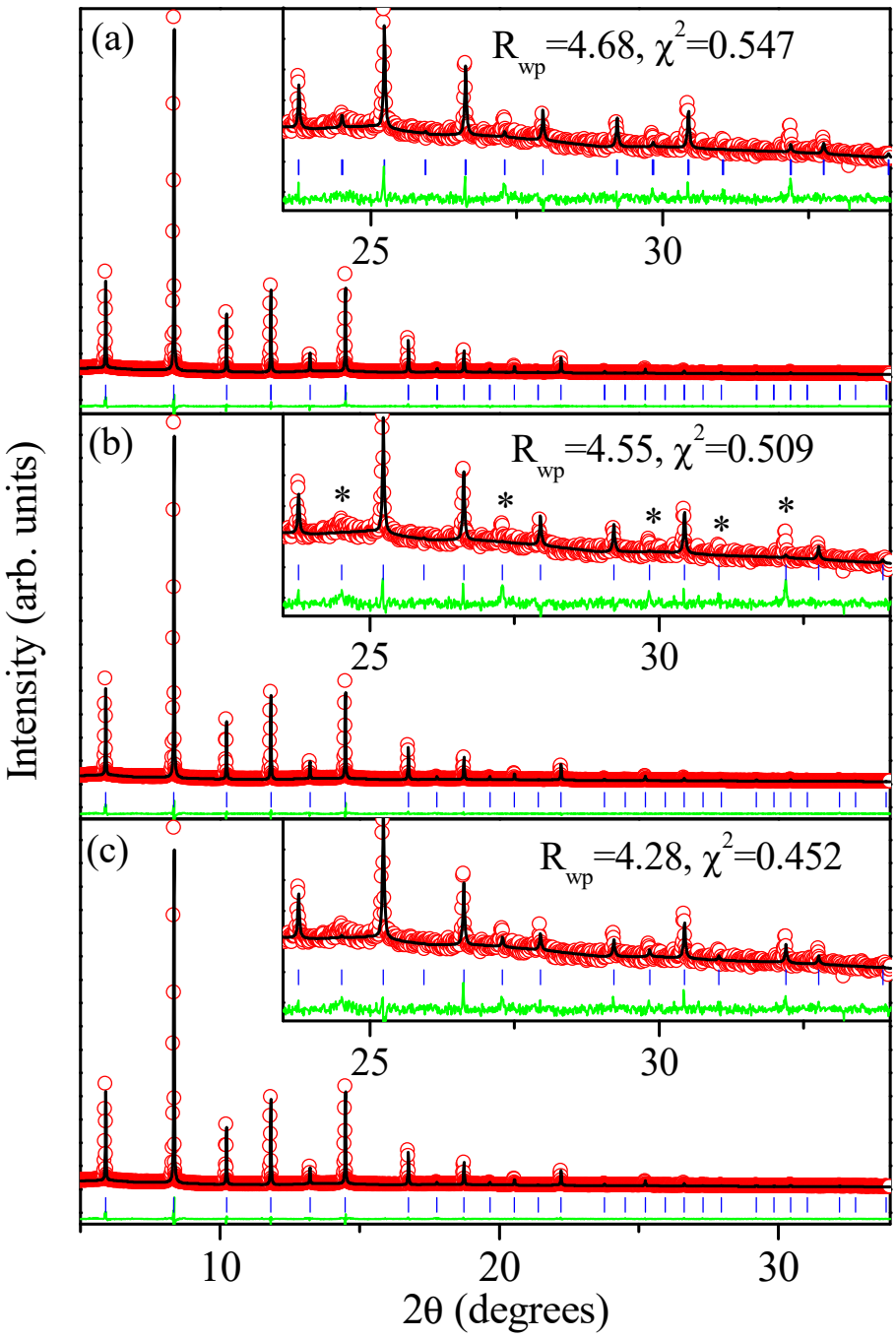

Fig. 4.6 Observed (dots), calculated (solid lines) and difference (bottom line) patterns obtained from the Rietveld analysis of the room temperature synchrotron x-ray diffraction data of BF-0.4PFN by using (a) P4mm, (b) $Pm\bar{3}m$ and (c) $Pm\bar{3}m$ with A-site & O-site local disorder models. The vertical tick marks above the difference pattern stand for the Bragg peak positions. The inset depicts the fit for high-angle reflections on a magnified scale. The peaks with h+k+l = odd in (b) are marked with an asterisk (*).

4.3.3.3 Local structure 'cubic' phase of BF-0.40PFN

As said earlier the huge value for the isotropic thermal parameters are common for the Pb-based perovskites and are well known in the literature, and are usually ascribed to local disordered displacements. The local structure refinement of Bi^{3+}/Pb^{2+} and O^{2-} ions was carried out using following steps: (i) We first fixed the O^{2-} ions at their ideal cubic position (1/2, 1/2, 0) and determined the true position (global minima in R_{wp}) of Bi^{3+}/Pb^{2+} ions using different local disorder models. (ii) We then fixed the Bi^{3+}/Pb^{2+} ions at their true position, and determined the true position of O^{2-} ions using different local disorder models. (iii) Finally, we kept the Bi^{3+}/Pb^{2+} and O^{2-} ions at their true positions and refined simultaneously their positions with isotropic thermal parameters. This procedure commonly used procedure to determine the true positions of ions corresponding to the lowest value of R_{wp}. It consists of a series of refinements based on a particular model in which atomic displacements along particular directions were fixed but all other parameters were refined. In order to determine the true position of ions with high isotropic thermal parameter, we considered three off-centre displacement models for the Bi^{3+}/Pb^{2+} ions from their ideal cubic position (0, 0 ,0) without destroying the overall cubic symmetry: (i) changing 1a (0, 0, 0) site to 6e (x, 0, 0) site with occupancy 1/6, (ii) changing 1a (0, 0, 0) site to 12i (x, x, 0) site with occupancy 1/12 and (iii) changing 1a (0, 0, 0) site to 8g (x, x, x) site with occupancy 1/8 [Thomas et al. (1999), Noheda et al. (1999), Singh et al. (2013)]. These three local displacement models correspond to displacements of ions along $<100>_{pc}$,

$<110>_{pc}$ and $<111>_{pc}$. Fig. 4.7(a) depicts the variation of the weighted profile (R_{wp}%) parameters with local atomic displacements for Bi^{3+}/Pb^{2+} ions in the directions <100>, <110> and <111>.

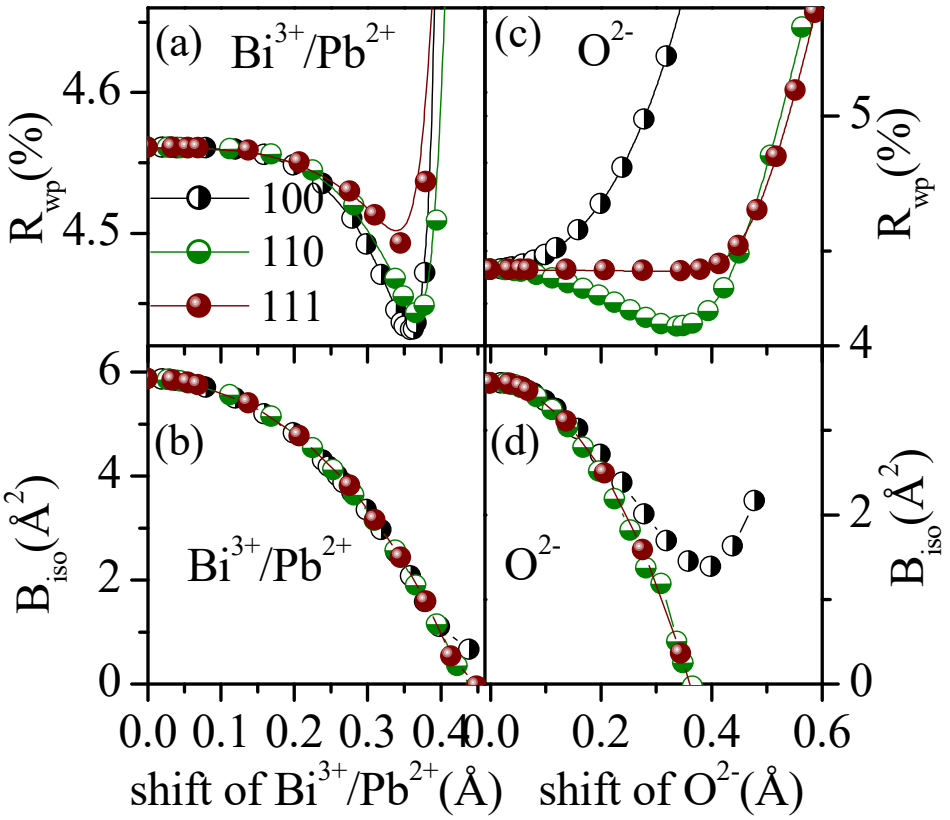

Fig. 4.7 Variation of weighted profile agreement factors R_{wp}(%) and thermal parameters B_{iso}(Å^2) with off- center displacement of (a) and (b) Bi^{3+}/Pb^{2+} and (c) and (d) O^{2-} for BF-0.4PFN.

The R_{wp} decreases with off-centre displacement of Bi^{3+}/Pb^{2+} ions along <100>, <110> and <111> directions but lowest minima was found in the <100> direction for x ~ 0.347 Å. Concomitantly, the isotropic thermal parameter B_{iso} for Bi^{3+}/Pb^{2+} also decreases with off-centre displacement of Bi^{3+}/Pb^{2+} ions along all the three off centre directions. We conclude that the local disorder of

Bi^{3+}/Pb^{2+} along <100> gives the best result with lowest R_{wp} = 4.48 % and B_{iso} = 2.24 $Å^2$. Rietveld refinement with A-site local disorder gives better fit with lower isotropic thermal parameter for the Bi^{3+}/Pb^{2+} atoms but O^{2-} site still have very high isotropic thermal parameter B_{iso} = 3.56 $Å^2$. Therefore, we also considered the local displacement of O^{2-} ion with respect to its special Wyckoff positions. Fig. 4.7(c & d) depict the variation of the R_{wp} and B_{iso} with the off-centre displacement of O^{2-} ion along the <100>, <110> and <111> directions. For O^{2-} ion, we observe a well-defined minimum in the weighted profile agreement factor (R_{wp}) for displacement of oxygen along <110> (i.e. along the face diagonals of the cube) with respect to the (0.5, 0.5, 0) Wyckoff position as shown in Fig. 4.7(c). The displacement of O^{2-} ion along the <001> and <111> directions does not reveal any minima as can be seen from Fig. 4.7(c). This confirms that O^{2-} is displaced along $<110>_{pc}$ direction.

In spite of the off-centering of Bi^{3+}/Pb^{2+} along <001> by 0.347 Å, the anisotropic thermal parameter of Bi^{3+}/Pb^{2+} along the [110] direction are still larger than that in the [001] direction ($\beta_{11} = \beta_{22} = 0.0345$, $\beta_{33} = 0.027$). More significantly, the equivalent isotropic thermal parameter B_{eq} =2.04 $Å^2$ is still quite high. This indicates that in addition to off-centering of Bi^{3+}/Pb^{2+} along the <001> direction, there is the possibility of off-centering of Bi^{3+}/Pb^{2+} along the x and y directions as well. We therefore considered the off-centered displacement of equal magnitude (to preserve the average cubic symmetry) along the x and y directions i.e. the <110> direction also, in addition to Bi^{3+}/Pb^{2+} and O^{2-} local displacements along the <001> and <110> direction,

respectively, in the refinements [Singh et al. (2013)]. We find that there is only a small improvement in the fit with a decrease in R_{wp} by 2% (i.e., from 4.48 to 4.28) for off-centered displacement of Bi^{3+}/Pb^{2+} (d ~ 0.098 Å) along the <110> direction. The amplitude of the thermal parameter of Bi^{3+}/Pb^{2+} becomes isotropic and drops to 1.98 $Å^2$ from the larger value of 2.24 $Å^2$. We thus conclude that Bi^{3+}/Pb^{2+} goes off-center from the cube corner positions like (0,0,0) to (x,x,z) positions while O^{2-} shifts from the center of the face (0.5,0.5,0) to (y,y,0) positions. The (x,x,z) and (y,y,0) positions correspond to general Wyckoff sites 24m and 12i respectively. So our refinements using high-energy synchrotron x-ray powder diffraction data reveal the occupancy of some of the general positions in the average cubic structure.

Fig.4.6(c) depicts the Rietveld fit for synchrotron x-ray diffraction data of BF-0.4PFN using Bi^{3+}/Pb^{2+} and O^{2-} at positions (x,x,z) and (y,y,0), respectively. The fit between the observed and calculated profiles has improved significantly, as can seen from the comparison of the inset to Fig. 4.6(b) with that in Fig. 4.6(c) with reduction in χ^2 from 0.509 to 0.452. In a similar way, we have analyzed the synchrotron x-ray diffraction data for other cubic compositions in the range $0.40 \leq x \leq 0.70$. The results of the Rietveld refinement are given in Table 4.1. We find that the off-center displacement of Bi^{3+}/Pb^{2+} along <001> (z direction in the present case) decreases with increasing Pb^{2+} content, while it increases along <110> (x and y directions) with increasing x. The values of x and z for different compositions are given in Table 4.1. The off-center displacement of O^{2-} along <yy0> is of the same

order of magnitude as compared that for Bi^{3+}/Pb^{2+} along <xxz> and it decreases with increasing x drastically. For example the off-center displacement of O^{2-} and Bi^{3+}/Pb^{2+} are ~ 0.34 Å and ~ 0.36Å along <yy0> and <xxz>, respectively, for BF-0.4PFN.

4.3.3.4 Local structure of BF-0.80PFN

The abrupt change in width of the 400_{pc} peak for $0.80 \leq x \leq 0.90$ with respect to its value for $0.40 \leq x < 0.80$, indicates a change of local structure within the average cubic symmetry. Initially, Rietveld refinement of BF-0.8PFN was carried out by considering cubic structure with $Pm\bar{3}m$ space group, as discussed in the previous chapter. Isotropic thermal parameters (B_{iso}) were used for all the atomic sites. The isotropic thermal parameters obtained after refinement have got very high values for the Bi^{3+}/Pb^{2+} (B_{iso} = 5.6 $Å^2$) and O^{2-} (B_{iso} = 3.5 $Å^2$) ions while for Fe^{3+}/Nb^{5+} (B_{iso} = 1.6 $Å^2$) is not so high. Similar results were also found for the Rietveld refinement using the laboratory source x-ray diffraction data. In the synchrotron data, satisfactory fit between observed and calculated profiles is found only for the lower 2θ angle. The mismatch between observed and calculated profiles is observed for the higher 2θ angle and some reflections, like the one marked with asterisk in Fig. 4.8(a), are not accounted at all. The weighted profile parameter is R_{wp} = 5.19% and χ^2 = 1.36. The split-site refinement of BF-0.8PFN was carried out by using similar approach as applied for the BF-0.4PFN composition.

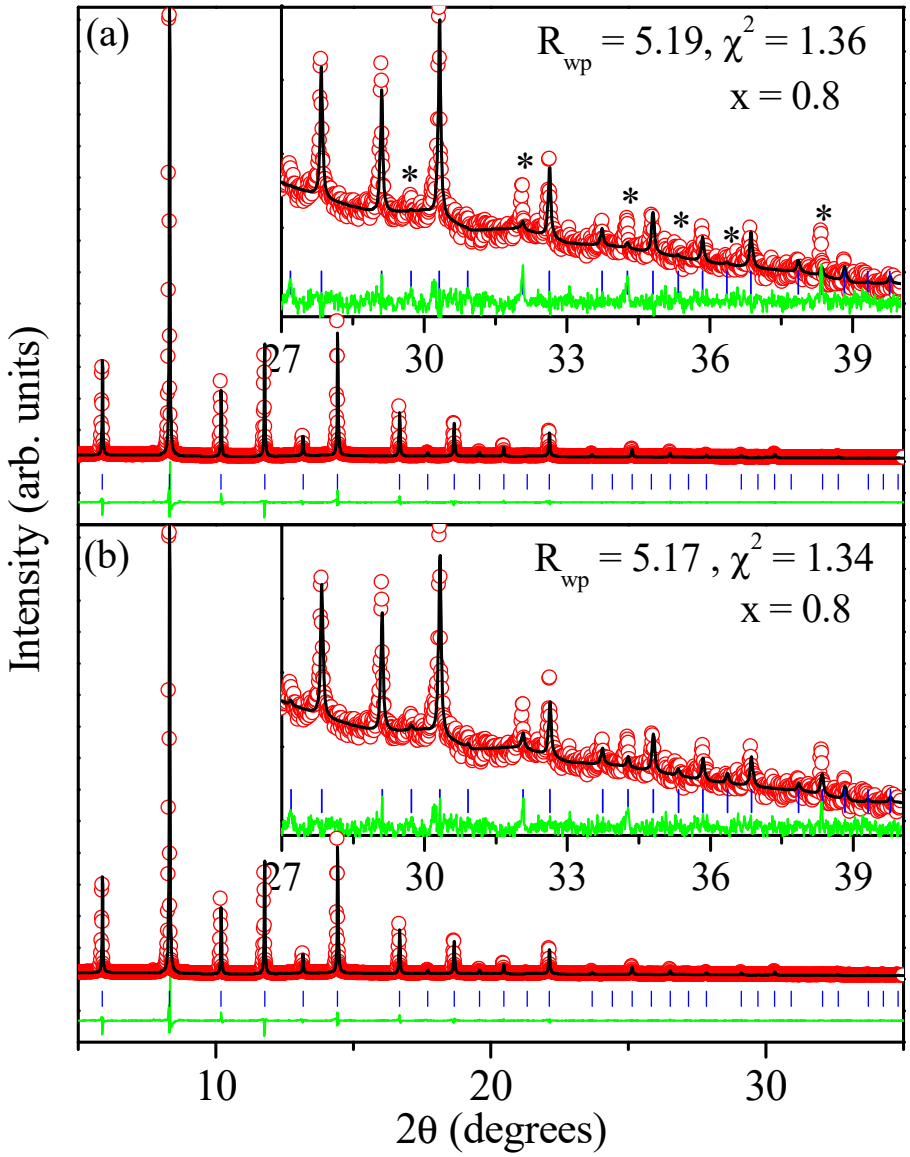

Fig. 4.8 Observed (dots), calculated (solid lines) and difference (bottom line) patterns obtained from the Rietveld analysis of the room temperature synchrotron x-ray diffraction data of BF-0.8PFN by using (a) $Pm\bar{3}m$ and (b) $Pm\bar{3}m$ with A-site & O-site local disorder models. The vertical tick marks above the difference pattern stand for the Bragg peak positions. The inset depicts the fit for high-angle reflections on a magnified scale.

Table 4.1 Rietveld refinement results of synchrotron x-ray diffraction data of BF-xPFN for x=0.30, 0.35, 0.40, 0.50, 0.70, 0.80, 0.90 and 0.96.

x	0.30	0.35	0.40	0.50	0.70	0.80	0.90	0.96
Space group	R3c a=b≠c, α=β=90°, γ=120°	R3c+Pm$\bar{3}$m	Pm$\bar{3}$m a=b=c, α=β=γ=90°					Cm a≠b≠c α≠β=90°≠γ
a (Å)	5.61921(7)	5.62537(2),3.9880	3.9914(6)	3.9968(5)	4.0032(4)	4.0064(7)	4.0098(6)	5.6725(3)
b (Å)	5.61921(7)	5.62537(2),3.9880	3.9914(6)	3.9968(5)	4 .0032(4)	4.0064(7)	4.0098(6)	5.6709(2)
c (Å)	13.8882(2)	13.8887(3),3.9880	3.9914(6)	3.9968(5)	4.0032(0)	4.0064(7)	4.0098(6)	4.0159(2)
β	90°	90°, 90°	90°	90°	90°	90°	90°	90.038(2)°
Bi/Pb (x)	0.0000	0.0000, 0.00	0.020(3)	0.022(2)	0.022(1)	0.0408(3)	0.0378(3)	0.0000
Bi/Pb (y)	0.0000	0.0000, 0.00	0.020(3)	0.022(2)	0.022(0)	0.0408(3)	0.0378(3)	0.0000
Bi/Pb (z)	0.2864(5)	0.2840(4), 0.00	0.088(2)	0.084(4)	0.075(1)	0.0408(3)	0.0378(3)	0.0000
Fe/Nb (x)	0.0000	0.0000, 0.50	0.50	0.50	0.50	0.50	0.500	0.501(1)
Fe/Nb (y)	0.0000	0.0000, 0.50	0.50	0.50	0.50	0.50	0.500	0.0000
Fe/Nb (z)	0.0139(5)	0.0139(2), 0.50	0.50	0.50	0.50	0.50	0.500	0.470(2)
O_I (x)	0.210(2)	0.211(4), 0.50	0.563(3)	0.543(2)	0.546(2)	0.527(3)	0.500	0.504(3)
O_I (y)	0.337(1)	0.348(4), 0.50	0.563(3)	0.543(2)	0.546(2)	0.527(3)	0.500	0.000
O_I (z)	0.0833	0.0833, 0.00	0.0000	0.0000	0.0000	0.0000	0.000	0.074(2)
O_{II} (x)	-	-, -	-	-	-	-	-	0.245(2)
O_{II} (y)	-	-, -	-	-	-	-	-	0.248(1)
O_{II} (z)	-	-, -	-	-	-	-	-	0.435(3)
B (Bi/Pb)	3.17(2)	3.02(2), 4.05(3)	1.98(2)	1.94(4)	2.07(3)	2.33(3)	2.09(3)	2.42(3)
B (Fe/Nb)	0.72(4)	0.85(3), 0.72(3)	1.29(6)	0.93(4)	0.88(4)	1.03(3)	1.01(4)	0.72(3)
B (O_I)	2.37(2)	2.23(4), 3.01(5)	1.8(3)	1.7(2)	1.8(1)	1.9(2)	2.7(3)	2.6(5)
B (O_{II})	-	-, -	-	-	-	-	-	1.2(2)
Fe-O_I	1.91796	1.96365,	2.027	2.0137	2.01876	2.0093	2.0049	2.0396
Fe-O_{II}	2.10960	2.06701,	2.027	2.0137	2.01876	2.0093	2.0049	1.9797
Fe-O-Fe	163.575	164.467,	161.40	162.97	169.95	174.02	180.0	174.51
R_{wp} (%)	3.78	3.67,	4.28	5.47	4.99	5.17	6.00	5.70
χ^2	0.62	0.68,	0.452	0.523	1.19	1.34	1.63	1.74

We consider the three off-centre displacement models for the Bi^{3+}/Pb^{2+} atoms from their ideal cubic position (0, 0 ,0) without destroying the overall cubic symmetry (i) 1a (0, 0, 0) site to the 6e (x, 0, 0) site with occupancy 1/6, (ii) 1a (0, 0, 0) site to the 12i (x, x, 0) site with occupancy 1/12 and (iii) 1a (0, 0, 0) site to the 8g (x, x, x) site with occupancy 1/8. Fig. 4.9(a) depicts the variation of the weighted profile (R_{wp}%) parameter with local atomic displacements for Bi^{3+}/Pb^{2+} ions in the <100>, <110> and <111> directions. The R_{wp} increases with off-centre displacement of Bi^{3+}/Pb^{2+} along the <100> direction while it decreases with off-centre displacement of Bi^{3+}/Pb^{2+} ions along the <110> and <111> directions and the lowest minima was found in the <111> direction for x ~ 0.29 Å and more significantly, the isotropic thermal parameter B_{iso} for Bi^{3+}/Pb^{2+} decreases with off-centre displacement of Bi^{3+}/Pb^{2+} ions along all the three off-centre directions as depicted in Fig. 4.9(b). Thus we conclude that the local disorder of Bi^{3+}/Pb^{2+} along <111> gives better fit with lowest R_{wp} = 5.17 % (χ^2=1.34) and B_{iso} = 2.33 $Å^2$. The anisotropic thermal parameters for Bi^{3+}/Pb^{2+} have got equal values i.e. $\beta_{11} = \beta_{22} = \beta_{33} = 0.036$ $Å^2$ which excludes the possibility of <xxz> type local displacement model for this composition, unlike that for $0.40 \leq x < 0.80$. After fixing the off-site local displacement for A-site ion, the B_{iso} for O^{2-} is still rather high. Therefore, we also considered the local displacement of O^{2-} in the refinement for the O^{2-} ion.

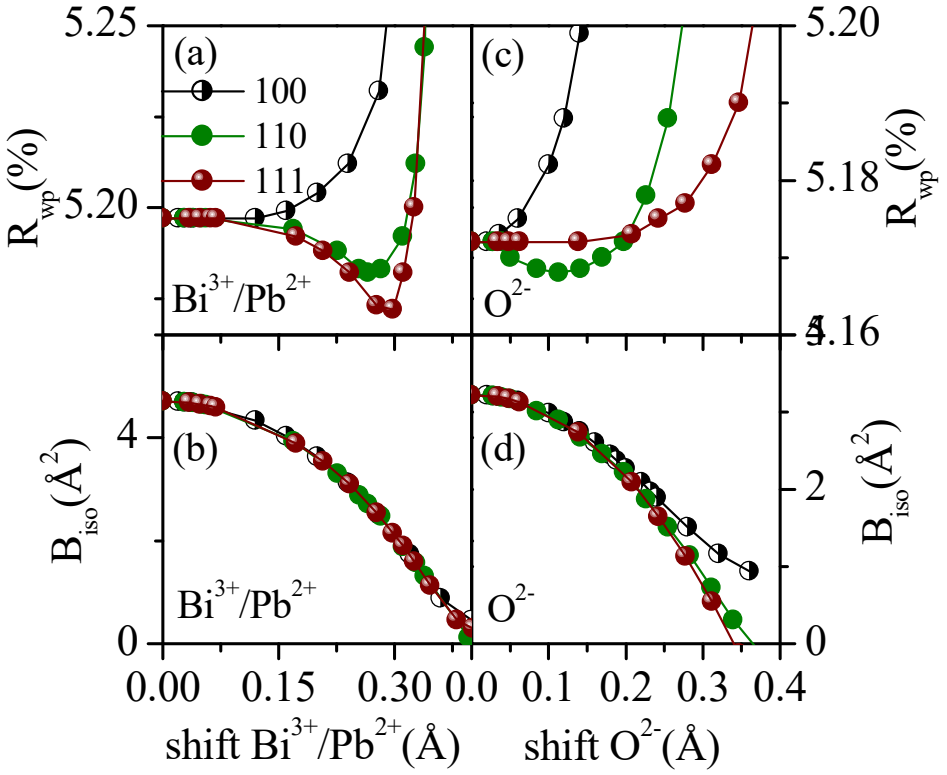

Fig. 4.9 Variation of weighted profile agreement factors R_{wp}(%) and thermal parameters B_{iso}(Å^2) with off-center displacement of (a) and (b) Bi^{3+}/Pb^{2+} and (c) and (d) O^{2-} for BF-0.8PFN.

Fig. 4.9(c) depicts the variation of R_{wp} with off-center displacement of O^{2-} along <100>, <110> and <111> directions. The variation of the R_{wp} with off-center displacement along <100> and <111> directions does not show any minima while a shallow minima (not well defined minima) is found along <110> direction, as can be seen in the Fig. 4.9(c). The isotropic thermal parameter (B_{iso}) decreases with off-center displacement along all the three directions of local displacement. We thus conclude that Bi^{3+}/Pb^{2+} goes off-

center from the cube corner positions (0,0,0) to (x,x,x) while O^{2-} shifts from center of the face (0.5,0.5,0) to (y,y,0) positions. The <x,x,x> and <y,y,0> positions correspond to general Wyckoff sites 8g and 12i. Therefore, we consider <xxx> local disorder model for Bi^{3+}/Pb^{2+} and <yy0> local disorder model for O^{2-} during the refinement. The nature of local disorder for Bi^{3+}/Pb^{2+} for BF-xPFN with x = 0.80 is thus different from that for $0.40 \leq x < 0.80$. Fig. 4.8(b) depicts the Rietveld fit between the observed and calculated profiles for the BF-0.8PFN compositions. The fit between the observed and calculated profiles does not show significant improvement, as can be seen by comparing the insets of Fig. 4.8(a) and Fig. 4.8(b). However, some of the reflections not accounted in the perfect cubic model (eg. the one marked with asterisk) are now accounted for. The Rietveld refinement of BF-0.9PFN was also carried out by considering the same local disorder model as used for BF-0.8PFN. However, local displacement is found only for Bi^{3+}/Pb^{2+} along <111> direction. We did not find any well defined local minima for the O^{2-} ions.

4.3.4 Variation of local displacement of Bi^{3+}/Pb^{2+} & O^{2-} with x

The local structure refinements reveal that A-site and O-site ions are not at their ideal cubic positions but they are displaced along <uuv> and <yy0> directions for the composition region $0.40 \leq x < 0.80$ and along <uuu> and <yy0> directions for the composition region $0.80 \leq x \leq 0.90$ respectively. However, for x = 0.90 composition the local disorder for O^{2-} is vanishingly small. Here, we also want to mention that Bi^{3+}/Pb^{2+} shows deepest local minima along <uuv> directions with local minima along <100>, <110> and

<111> directions for compositions with $0.40 \leq x < 0.80$ while Bi^{3+}/Pb^{2+} shows minima only along <110> (local minima) and <111> (global minima) directions for $x \geq 0.80$. Fig. 4.10 depicts the variation of the off-center displacement of A-site and O-site ions with composition (x). The off-center displacement along <00v> directions for Bi^{3+}/Pb^{2+} ions decreases linearly with increasing Pb^{2+} content while the off-center displacement along <uu0> direction increases with increasing Pb^{2+} content. Both become equal for $0.80 \leq x < 0.96$. The off-center displacement of O^{2-} ion along <110> decreases sharply with decreasing Bi^{3+} content and becomes approximatively zero for $x > 0.87$. The off-center displacement of O^{2-} ion for the compositions $x = 0.90$ is very small, if at all it is present, which cannot be determined accurately in the present experimental condition.

Noheda et al. [Noheda B. and Gonzalo J. A. (2000)] have given the relationships between the tetragonal, rhombohedral and monoclinic structures in terms of the local displacements. It has been shown that combination of tetragonal [001] shift with local <110> shift or rhombohedral [111] shift with local <001> shift gives monoclinic structure [Noheda B. and Gonzalo J. A. (2000)]. In the present study, Bi^{3+}/Pb^{2+} ions are locally displaced along <uu0> and <00v> directions with local O^{2-} displacement along <yy0> in the composition range $0.40 \leq x < 0.80$. The local displacement components of Bi^{3+}/Pb^{2+} ions along <uu0> and <00v> directions gives the local monoclinic distortion with Cm space group [Singh et al. (2013)]. The local displacement of O^{2-} along <yy0> is associated with the local octahedral tilt [Singh et al.

(2014)]. The combined effect of local displacement of Bi^{3+}/Pb^{2+} along <uu0> and <00v> directions with local displacement of O^{2-} along <yy0> gives the monoclinic distortion with locally Cc phase [Singh et al. (2013)]. Therefore, the first morphotropic phase boundary at $x_C = 0.40$ is due to R3c to locally Cc phase transition.

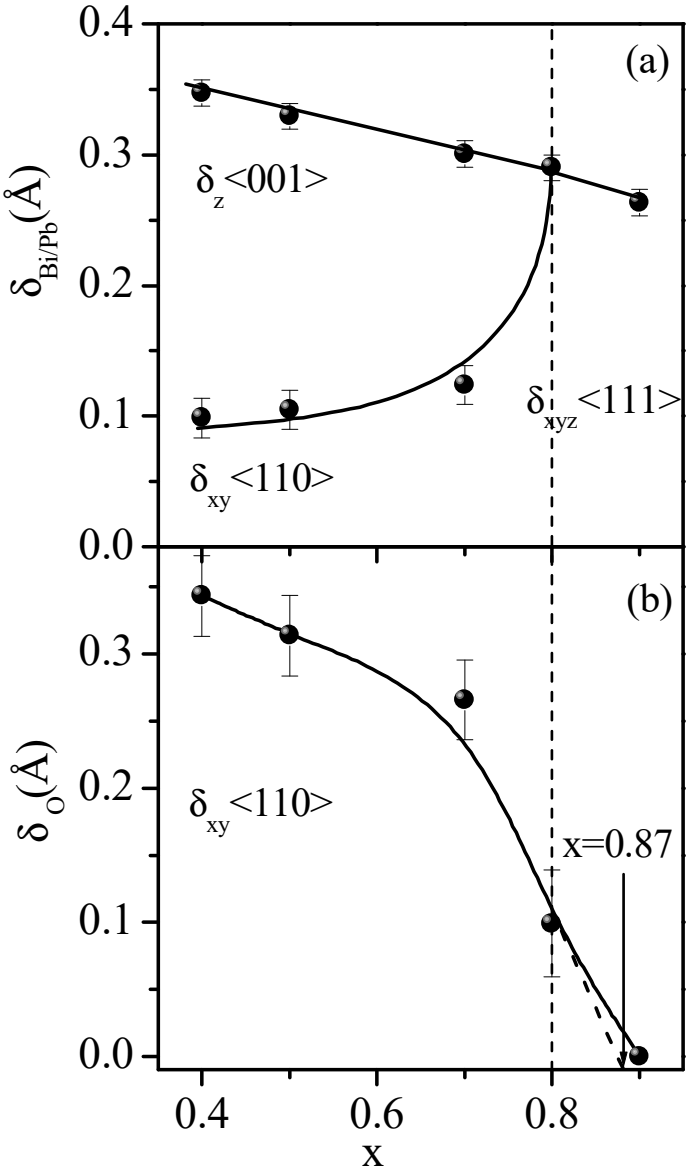

Fig. 4.10 Variation of off-center displacement of (a) Bi^{3+}/Pb^{2+} along <110> and <001> directions and (b) O^{2-} along <110> direction.

Since the local displacements of Bi^{3+}/Pb^{2+} along <uuu> are such that v >u, the monoclinic Cc phase can be said to be M_A type with octahedral tilt (for definition of M_A-type see Vanderbilt and Cohen (2001)). For the M_B phase with Cc space group u > v, this is not the case here. Our results show R3c to Cc phase transition in bulk powder which differs with the Cc-Cc phase transition in thin films [Zeches et al. (2009), Chen et al. (2011)]. The second morphotropic phase boundary exists at x = 0.80. The local displacement of the Bi^{3+}/Pb^{2+} ions along <uuu> for $x \geq 0.80$ can be defined in terms of the local rhombohedral distortions with R3m space group. Therefore, second morphotropic phase boundary is due to the locally Cc to locally R3m phase transition. With the present resolution of the synchrotron x-ray diffraction data, we did not find any weak monoclinic distortions but there might be the possibility for the existence of weak monoclinic distortion in BF-0.8PFN. It has been reported that the room temperature structure of $Pb(Fe_{0.5}Nb_{0.5})O_3$ is not rhombohedral with R3m space group [Ivanov et al. (2000)] but pseudorhombohedral/monoclinic with Cm space group [Lampis et al. (1999), Singh et al. (2007)]]. We have found $Pb(Fe_{0.5}Nb_{0.5})O_3$ like structure only for x > 0.90 composition. This implies that, the second MPB at $x_C = 0.8$ is due to local Cc to local R3m phase transition. The local R3m phase completely transforms into global Cm phase for x > 0.90 compositions.

4.3.5 Implications of local disorder of O^{2-} and Bi^{3+}/Pb^{2+}

4.3.5.1 Local oxygen octahedral tilt

In the rhombohedral (R3c) structure of $BiFeO_3$, the long range ferroelectric order arises from the polar displacements of 6a Wyckoff site ions along $[111]_{pc}$ and is accompanied with tilting of oxygen octahedra about $[111]_{pc}$ as well. As a result of $Pb(Fe_{0.5}Nb_{0.5})O_3$ substitution to in $BiFeO_3$, both the polar displacements and oxygen octahedral tilting angle decreases and vanishes in the average cubic structure with $Pm\bar{3}m$ space group for $0.40 \leq x \leq 0.90$, since we do not observe the superlattice peaks. However, Rietveld analysis of high energy synchrotron x-ray diffraction data for cubic compositions reveals local displacements of O^{2-} along $<110>_{pc}$ directions from their cubic special positions (0.5,0.5,0). The $<110>_{pc}$ displacements of O^{2-} are equivalent to the rotation of oxygen octahedra about $<111>_{pc}$ directions [Singh et al. (2013)]. Therefore, our results reveal that the rhombohedral phase of BF-xPFN looses its long range ordered octahedra tilt at the R3c to $Pm\bar{3}m$ transition, but this tilt persists locally beyond the phase transition composition ($x \geq 0.40$) even in the so-called cubic phase [Singh et al. (2013)]. The decrease in the displacement of O^{2-} with increasing x suggests that the local tilt disorder also decreases with decreasing Bi^{3+} content in BF-xPFN as expected. However, the local tilt completely disappears above the second MPB at $x \approx 0.87$.

4.3.5.2 Ferroelectric polarization due to local Bi^{3+}/Pb^{2+} disorder

In perovskite compounds with ABO_3 structure, the tilt of oxygen octahedra does not break the inversion symmetry, and no ferroelectricity can be observed due to tilting of oxygen octahedral. We can estimate the polarization direction due to off-center displacement of Bi^{3+}/Pb^{2+} along <uuv> in the average cubic structure using point charge approximation by the expression: $P = (1/V)\Sigma_i q_i r_i$, where V is the volume of the unit cell and q_i is the charge on the i^{th} atom with position vector r_i in the unit cell from the centrosymmetric position [Hewat (1973), Singh et al. (2013)]. The calculated ionic polarization obtained from the local Bi^{3+}/Pb^{2+} disorder positions for two MPBs composition at x = 0.40 and x = 0.80 are found to be ~ 37.56 $\mu C/cm^2$ and ~ 34.27 $\mu C/cm^2$. Since our BF-xPFN samples are semiconducting we could not measure *P-E* loops. However, Paik et al. have reported the *P-E* loops for La doped samples of BF-0.7PFN and BF-0.8PFN. The saturation polarization was reported to be ~ 0.27$\mu C/cm^2$ and ~ 1.41$\mu C/cm^2$ for La doped BF-0.7PFN and BF-0.8PFN compositions respectively which are much lower than our calculated ionic polarization.

4.3.5.3 Local monoclinic distortion of M_A-type and rotation of polarization vector

The room temperature crystal structure of end compositions of BF-xPFN solid solution is R3c and Cm (pseudorhombohedral). Both the end members are ferroelectric and their polarization directions are confined along

<111> and <uuu> direction. The R3c phase of BF-xPFN transforms into the locally disordered structure at x = 0.40 for which Bi^{3+}/Pb^{2+} ions are displaced along <uuv> directions characteristics of the M_A-type monoclinic phase. It transforms into the R-like phase at the second MPB x = 0.80. We have calculated the angle of rotation (θ) of the polarization vector as a function of $Pb(Fe_{0.5}Nb_{0.5})O_3$ content (x) from the magnitude of the local Bi^{3+}/Pb^{2+} displacement. The variation of the angle of rotation with x is shown in Fig. 4.11 and the corresponding polarization vectors in the Cohen's cube shown in Fig. 4.12 for various values of x. Our results suggest that BF-xPFN is of M_A-type monoclinic, whose polarization vector is confined in (1-10) plane.

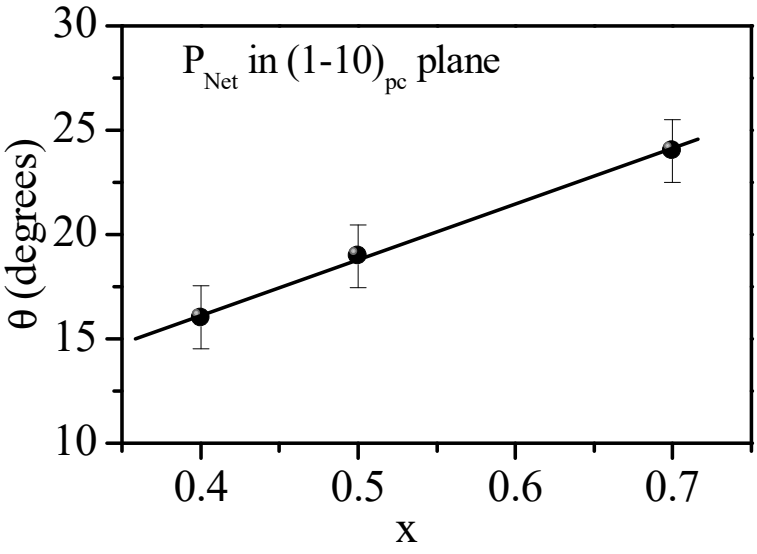

Fig. 4.11 Variation of the polarization angle with respect to the [001] direction on the $(1\text{-}10)_{pc}$ plane with x for various pseudocubic compositions of BF-xPFN with x = 0.4, 0.5 and 0.7.

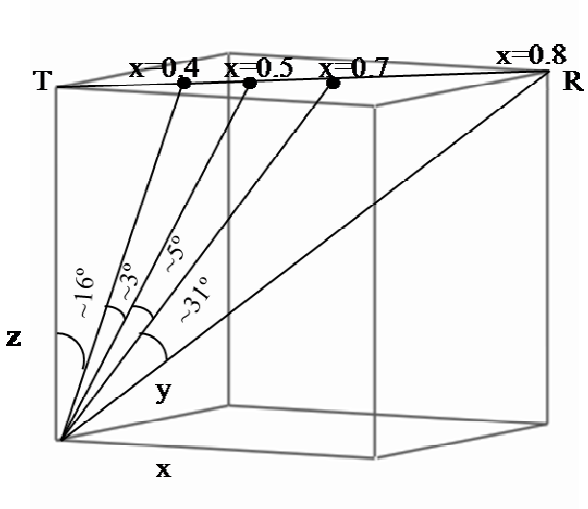

Fig. 4.12 Schematic depiction of rotation of polarization vector from R to T phases in BF-xPFN (R-M_A-T).

The polarization vector continuously changes direction from a direction chosen to $[001]_{pc}$ at the Bi-excess end to the $[111]_{pc}$ direction (Bi-deficient end) on increasing x as shown in Fig. 4.14. BF-xPFN thus shows R (global R3c)-M_A(local Cc)-R(local R3m) type of structural phase transition with composition. We did not find the occurrence of the M_C and M_B type of monoclinic phases in BF-xPFN solid solution proposed by Vanderbilt and Cohen with [uvw] and [uuv], u <v type local displacements. In the $Pb(Zr_xTi_{1-x})O_3$ (PZT) and $(1-x)BiFeO_3$-$xBaTiO_3$ (BF-xBT) ceramics, R- M_A-T type of polarization rotation has been reported. The M_A type of monoclinic phase acts as bridging phase between the rhombohedral and tetragonal phases [Noheda (2006), Singh (2013)]. The PMN-xPT and PZN-xPT ceramics show R- M_B-M_C-T structural path with M_B(Cm) and M_C(Pm) type phases as bridging

phases [Singh and Pandey (2003)]. The stress induced R- M_A - M_C -T path was also reported for the pure $BiFeO_3$ thin films [Christen et al. (2011)].

4.3.5.4 Variation of the structural parameters with composition

Fig. 4.13 depicts the variation of the lattice parameter, unit cell volume and thermal parameters with composition for the synchrotron x-ray diffraction data. A few data points where synchrotron data was not available, we have included laboratory XRD data based results in Fig. 4.13 (a) and (b). For clarity, B_{iso} is plotted only for the synchrotron x-ray diffraction data. The unit cell parameters and volume plot with x follow nearly the same trend as obtained from the laboratory x-ray diffraction data. The magnitude of B_{iso} obtained from the local displacements in the average cubic compositions of BF-xPFN for Bi^{3+}/Pb^{2+} and O^{2-} ions are smaller in comparison with the values obtained from the x-ray diffraction data without local displacements. The Rietveld refinement of the laboratory x-ray diffraction data gives evidence for two MPBs at x=0.40 and x=0.90. The first MPB is due to the R3c to cubic phase transition and second MPB is due to the cubic to monoclinic phase transition. The local structure refinement using synchrotron x-ray diffraction data reveals that the $0.40 \leq x < 0.80$ compositions are locally monoclinic with Cc space group type displacements while the compositions with $0.80 \leq x < 0.90$, the structure is locally rhombohedral with R3m space group.

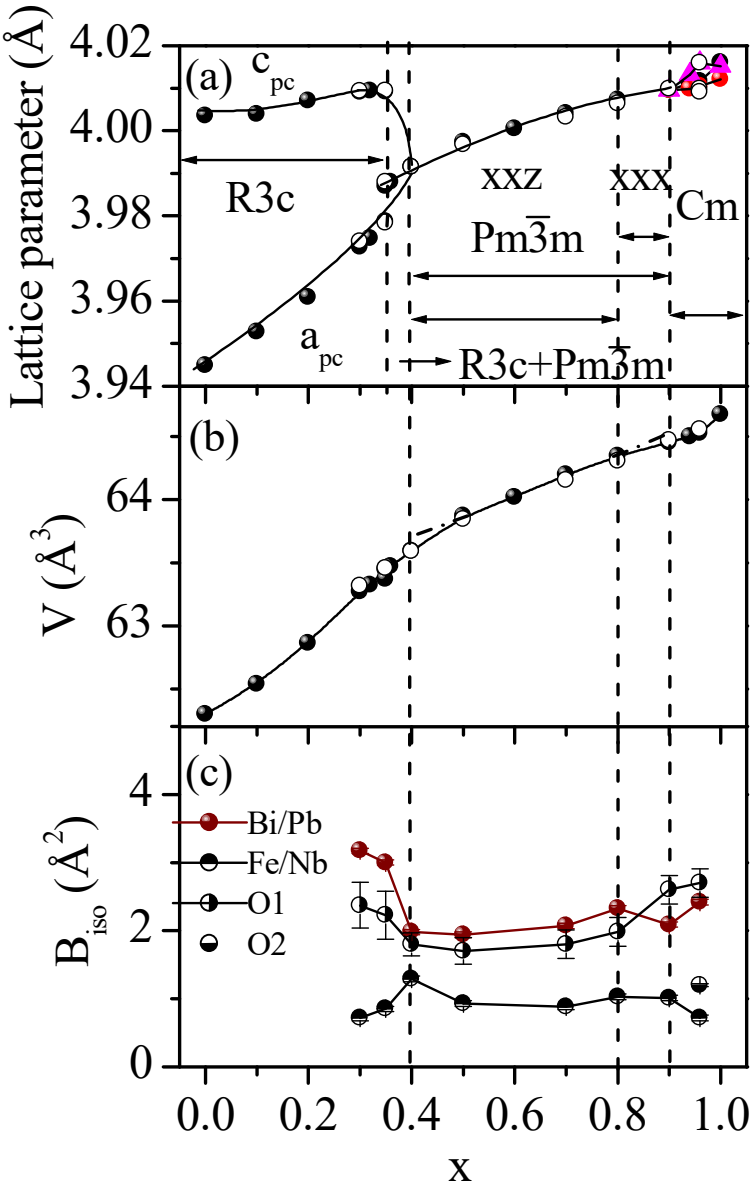

Fig. 4.13 Composition variation of (a) refined pseudocubic lattice parameter (b) pseusocubic unit cell volume (c) isotropic thermal parameters for the Bi^{3+}/Pb^{2+}, O^{2-}, and Fe^{3+}/Nb^{5+} ions. Dots in (a) and (b) are due to the x-ray data while the circles are due to the synchrotron x-ray diffraction data. For clarity only synchrotron data are plotted for the thermal parameter after local structure refinement.

This shows that the second MPB is not at x = 0.90 composition but it is located at x~0.80 composition. The second MPB is due to the local Cc to local R3m phase transition. The local R3m phase transforms into a global Cm phase for x>0.90 compositions.

4.3.6 Evidence for morphotropic phase boundaries (MPBs): room temperature dielectric study

Figure 4.14 depicts the composition dependence of dielectric (ε_r') constant for BF-xPFN solid solution. The dielectric constant (ε_r') for $BiFeO_3$ was taken from Kumar and Palkar (2000). The dielectric constant initially increases slightly up to x = 0.10 composition for which we have found the maximum values of remanent magnetization to be discussed in chapter VII. The maximum values of the remanent magnetization for x = 0.10 composition are due to the melting of the spiral spin ordering and hence release of the locked-in magnetization by doping effects. The weak anomaly in dielectric constant at x = 0.10 composition indicates the coupling of the magnetic and ferroelectric order parameters. The details of the magnetoelectric coupling will be discussed in chapter VIII. The dielectric constant for the composition x > 0.10 decreases with increasing x up to the x=0.30 composition. For the x > 0.30 compositions, the dielectric constant continuously increases with increasing x with a small hump at x = 0.40 and a huge dielectric peak at x = 0.80 compositions. The dielectric anomaly at x = 0.40 indicates the first morphotropic phase boundary due to the R3c to average cubic (locally Cc)

phase transition. The huge dielectric anomaly at x = 0.80 is due to the structural phase transition within the average cubic structure due to change of local disorder of Bi^{3+}/Pb^{2+} along <xxz> (locally Cc) to that along <xxx> (locally R3m).

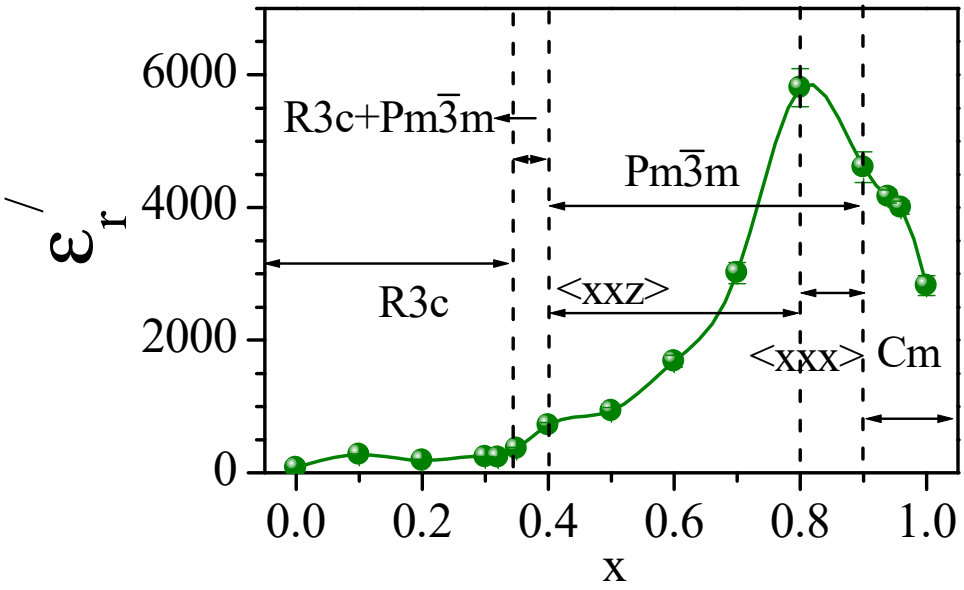

Fig. 4.14 Variation of the real part of the dielectric constant (ε_r') of BF-xPFN solid solutions with x at room temperature.

The very high value of the dielectric constant is also reported in literature for PFN end compositions in comparison to the BF end compositions. For example the dielectric constant (ε_r' at T = 300 K) of 0.8BLF-0.2PFN was reported to be ~ 300 while those of 0.3BLF-0.7PFN and 0.2BLF-0.8PFN were reported to be order of ~ 10^3 [Paik et al. (2009)]. The dielectric constant for x >0.80 decreases with increasing x with a hump at x = 0.94 composition indicates the average cubic (R3m locally) to the monoclinic phase (Cm phase globally) transition.

Therefore, our room temperature dielectric plot reveals all the composition dependent structural phase transition using laboratory x-ray and high resolution synchrotron x-ray diffraction data.

4.4 Summary and conclusions

The room temperature crystal structure for different compositions of BF-xPFN has been settled by using high energy synchrotron x-ray diffraction data. The anomalously high values of isotropic thermal parameters for the A-site and O-site ions in the cubic phase are resolved by their local structure refinements. The local structure refinement in the cubic phase of BF-xPFN shows that Bi^{3+}/Pb^{2+} and O^{2-} ions are not at their ideal cubic position but they are displaced along <uuv> ($v > u$ for $x < 0.8$ and $v \approx u$ for $x \geq 0.8$ composition) and <yy0> directions respectively. The true crystal structure at local level is found to be monoclinic. Present study, demonstrates the evidence for two MPBs for the BF-xPFN solid solution. The R3c to locally Cc phase transition occurs at the first MPB at $x \approx 0.40$ while the locally Cc to R3m phase transition occurs at the second MPB at $x = 0.80$. The R-M_A-R type of polarization rotation path occurs with x for the BF-xPFN solid solutions. The presence of structural phase boundaries is further confirmed by the room temperature dielectric plot. The composition dependent dielectric plot exhibits two peaks at $x = 0.40$ and $x = 0.80$ compositions which correspond to the two MPBs of the BF-xPFN system. A hump in dielectric constant plot at $x \sim 0.94$ indicates the average cubic with local R3m to the monoclinic phase (Cm phase) transition.